Journal of Materials Chemistry C

Accepted Manuscript

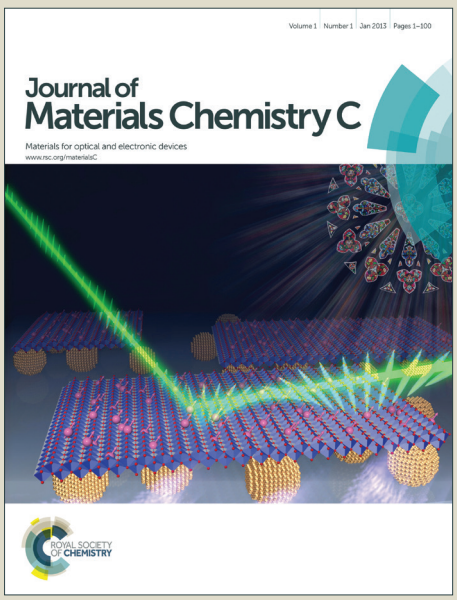

ROYAL SOCIETY OF CHEMISTRY

www.rsc.org/materialsC

Journal of Materials Chemistry C

RSCPublishing

PAPER

$CaY_2Si_2S_8:Ce^{3+}$: A novel green-emitting thiosilicate phosphor for white light-emitting diodes

Cite this: J. Mater, Chem, C,2014, 7, X

Szu-Ping Lee,[a] Chien-Hao Huang,[b] and Teng-Ming Chen*[a]

Received 00th July 2014
Accepted 00th July 2014

DOI: 10.1039/x0xx00000x

www.rsc.org/MaterialsC

A novel green-emitting Ce^{3+}-doped $CaY_2Si_2S_8$ thiosilicate phosphor was synthesized by using solid-state methods in a sealed silica ampoule. This compound could be excited over a broad range from UV to blue light (400−450 nm) and generated a broadband emission peaking at ~495 nm, with a quantum efficiency of ~57%, which are promising for solid-state lighting applications. Temperature-dependent optical measurements of $CaY_2Si_2S_8:Ce^{3+}$ from 25 to 225°C were performed. In addition, a white LED device was fabricated by using the green-emitting $CaY_2Si_2S_8:Ce^{3+}$ phosphor and red-emitting $CaAlSiN_3:Eu^{2+}$ commodity pumped with a 450 nm blue chip. The CRI value and CCT were measured to be 91–95 and 3800–8600 K, respectively, showing promising potential for solid-state lighting applications. The preparation, spectroscopic characterization, quantum efficiency, decay lifetime, thermal stability, and related LED device data are also presented.

1. Introduction

In recent years, solid-state white-light devices have been championed as next-generation light sources because of their advantages of long operation lifetime and energy efficiency.[1–5] Moreover, they have environmental merit because they do not contain mercury vapor as a light source.[6] White light can be produced by a combination of a blue LED chip with a yellow-emitting phosphor.[4,7–12] However, such white light has some disadvantages such as low color-rendering index (CRI) and high correlated color temperature (CCT) due to the deficiency of red emission.[7,8] An alternative way to produce white with a high CRI may be based on a combination of a near-ultraviolet (near-UV) LED chip (380−420 nm) with red-, green-, and blue-emitting phosphors.[7–10] With the aim of realizing the optical requirements for white light, many new phosphors have been developed to overcome the aforementioned drawbacks and obtain suitable luminescent material for phosphor-converted white light-emitting diodes (pc-WLEDs).[7–10] Ce^{3+} emission usually consists of a broad band due to the parity-allowed transition between the lowest crystal field components of the 5*d* excited state and the 4*f* ground states ($^2F_{7/2}$ and $^2F_{5/2}$), and it often extends from the UV to yellow region, depending on the host lattice.[13–16]

Phosphor materials including silicates and rare-earth ions have been studied for use in various light sources and displays. Up to now, silicate, silicon nitride, silicon oxynitride, and thiosilicate materials have been reported.[17–29] In particular, thiosilicate phosphors have the advantage that a relatively low temperature is necessary for fabrication, and various luminescence wavelengths from blue to infrared have been reported.[17,21–29] From these viewpoints, the fabrication of a visible and infrared thiosilicate phosphor is expected. In this research, we discovered a new Ce^{3+}-activated $CaY_2Si_2S_8$ thiosilicate phosphor, which crystallizes in the $Ce_2PbSi_2S_8$[30] structure. For the first time, we investigated the crystal structure of the $CaY_2Si_2S_8:Ce^{3+}$ via synchrotron X-ray diffraction (SXRD) patterns and reported the luminescent properties of the $CaY_2Si_2S_8:Ce^{3+}$ phosphor. This new phosphor can be excited by light in the near-UV to blue region and shows green emission. In addition, the LED device using the $CaY_2Si_2S_8:Ce^{3+}$ phosphor with a blue LED chip was investigated to demonstrate the applicability of the $CaY_2Si_2S_8:Ce^{3+}$ phosphor as a color-conversion material in the fabrication of WLEDs.

2. Experimental Section

2.1. Materials and synthesis

The powder samples of $Ca(Y_{1-x}Ce_x)_2Si_2S_8$ were synthesized by solid-state reactions using Y_2S_3 (Alfa, 99.9%), CaS (Alfa, 99.9%), Ce_2S_3 (Alfa, 99.99%), Si powder (Alfa, 99.999%), and S powder (Acros, 99.999%) as raw materials. The stoichiometric amounts of the starting materials were thoroughly mixed and loaded into a vertically positioned silica ampoule, fully evacuated to 10^{-3} Torr, and sealed off under a dynamic vacuum. The silica ampoule was heated at 5 °C/min to 1000 °C for 8 h in a furnace and then cooled down slowly to room temperature.

2.2. Characterization

The SXRD profiles were recorded at the BL01C2 beamline of National Synchrotron Radiation Research Center (NSRRC) in Hsinchu, Taiwan, equipped with a Mar345 imaging plate and using an X-ray wavelength of 0.774908 Å. X-ray absorption parameters and the extinction coefficient were also refined, moreover, the peak shapes were fitted using exponential pseudo-Voigt functions. The diffuse reflection (DR) spectra were measured with a Hitachi 3010 double-beam UV−Vis spectrometer (Hitachi Co., Tokyo, Japan) equipped with a ø60 mm integrating sphere whose inner face was coated with $BaSO_4$ or Spectralon and α-Al_2O_3 was used as a standard in the measurements in the range of 250−800 nm. The

photoluminescence (PL) and photoluminescence excitation (PLE) spectra were recorded with a Spex Fluorolog-3 spectrofluorometer (Jobin Yvon Inc./specx) equipped with a 450 W Xe lamp and analyzed by a Jobin-Yvon spectrometer HR460 with multichannel charge-coupled device detector. The absorption (A) and quantum efficiency (QE) was measured by an integrating sphere whose inner face was coated with Spectralon equipped with a spectrofluorometer (Horiba Jobin-Yvon Fluorolog 3−2−2). The luminescence decay lifetime were measured on a tunable nanosecon optical-parametric-oscillator/Q-switch-pumped YAG:Nd^{3+} laser system (Ekspla). The thermal luminescence (TL) quenching was tested using a heating apparatus (THMS-600) in combination with PL equipment. The pc-WLEDs devices were fabricated using commercial blue InGaN-based LED chips (λ_{max} = 450 nm) with an intimate mixture of silicone resin and phosphor blending of green-emitting $CaY_2Si_2S_8:Ce^{3+}$, and red emitting $CaAlSiN_3:Eu^{2+31}$ commodities (Mitsubishi-BR-102C). The electroluminescence (EL) spectra were recorded at different forward bias currents in the range of 150−850 *m*A and measured by SphereOptics integrating sphere with LED measurement starter packages (Onset, Inc.). The Commission Internationale de l'Eclairage (CIE) chromaticity coordinates were determined by a Laiko DT-100 color analyzer equipped with a CCD detector (Laiko Co., Tokyo, Japan).

3. Results and Discussion

3.1. Structure Characterization of the $Ca(Y_{1-x}Ce_x)_2Si_2S_8$ Thiosilicate Phosphor

Figure 1 shows the SXRD patterns of the as-synthesized $Ca(Y_{0.93}Ce_{0.07})_2Si_2S_8$ sample and the ICSD_184024 standard pattern. The as-synthesized $Ca(Y_{0.93}Ce_{0.07})_2Si_2S_8$ sample was obtained as a single-phased compound that matches well with ICSD file No. 184024. $Ca(Y_{0.93}Ce_{0.07})_2Si_2S_8$ synthesized in this study was found to crystalize trigonally in *R*-3*c* (No. 167) with six formula units per unit cell. In the crystal lattice and unit cell of $Ca(Y_{0.93}Ce_{0.07})_2Si_2S_8$, there is a single site randomly occupied by a mixture of Ca and Y atoms, one site occupied by the Si atoms, and two sites occupied by chalcogen atoms. The Si and S atom sites are fully occupied.[32] Figure 2 shows the exact crystal structure of $Ca(Y_{0.93}Ce_{0.07})_2Si_2S_8$ lattice viewed along the *c*-axis and Ca/Y atomic site with their corresponding neighboring atoms from the refined results. Generally, the atomic framework consists of $[(1/3Ca + 2/3Y)S_8]$ bicapped trigonal prisms and $[SiS_4]$ tetrahedra, which are mutually connected by corners and edges.[32] The coordination polyhedron of Ca/YS_8 is composed of eight S and one Ca/Y atoms situated at the center of the bicapped trigonal prism with a coordination number (CN) of 8.

3.2. Spectroscopic Characterizations of the $Ca(Y_{1-x}Ce_x)_2Si_2S_8$ Thiosilicate Phosphor

Figure 3 shows the DR spectrum of as-synthesized polycrystalline $CaY_2Si_2S_8$ and $Ca(Y_{0.93}Ce_{0.07})_2Si_2S_8$. For the $CaY_2Si_2S_8$ host, the DR spectrum shows high reflection in the wavelength ranging from 400 to 800 nm, and decreases the reflection intensity from 250 to 450 nm. When 7% Ce^{3+} is induced into the $CaY_2Si_2S_8$ host lattice, the absorption edge extends to the longer-wavelength side and the absorption is enhanced. The observed results suggest two different absorption pathways from the UV to visible range: one is caused by the $CaY_2Si_2S_8$ host and the other is caused by the $4f^1 \rightarrow 5d^1$ transitions of the Ce^{3+} ion. A typical PLE/PL spectrum of $Ca(Y_{0.93}Ce_{0.07})_2Si_2S_8$ is indicated in Figure 3 (b).

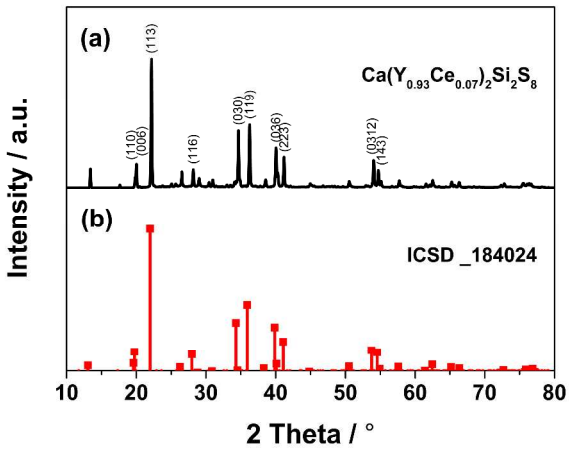

Figure 1 SXRD patterns of (a) as-synthesized $Ca(Y_{0.93}Ce_{0.07})_2Si_2S_8$ sample and (b) ICSD_184024.

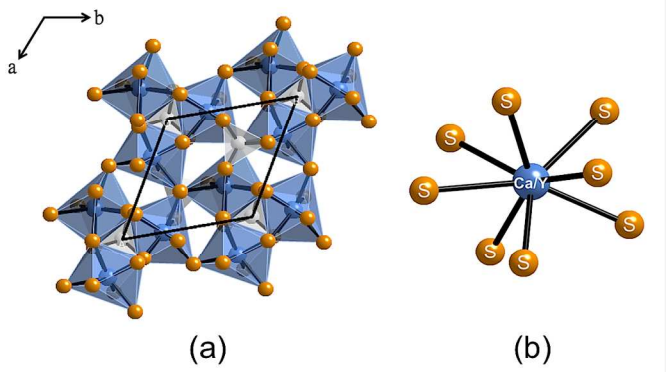

Figure 2 (a) Schematic unit cell crystal structure of $Ca(Y_{0.93}Ce_{0.07})_2Si_2S_8$ viewed along the *c*-axis and (b) coordination environment around Ca/YS_8. Green, yellow and white sphere balls describe Ca/Y/Ce, S and Si atoms.

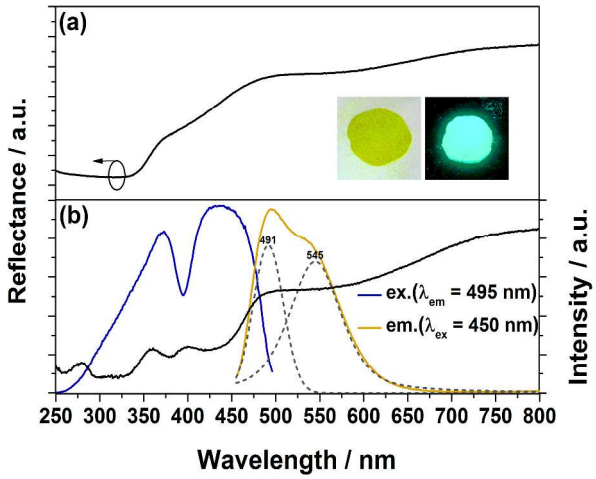

Figure 3 (a) DR spectrum of $CaY_2Si_2S_8$ host. (b) DR spectrum, PLE/PL spectra, and the PL deconvolution (dashed line) of $Ca(Y_{0.93}Ce_{0.07})_2Si_2S_8$. The insets show photographs of the synthesized phosphor under room light (left) and UV light (right).

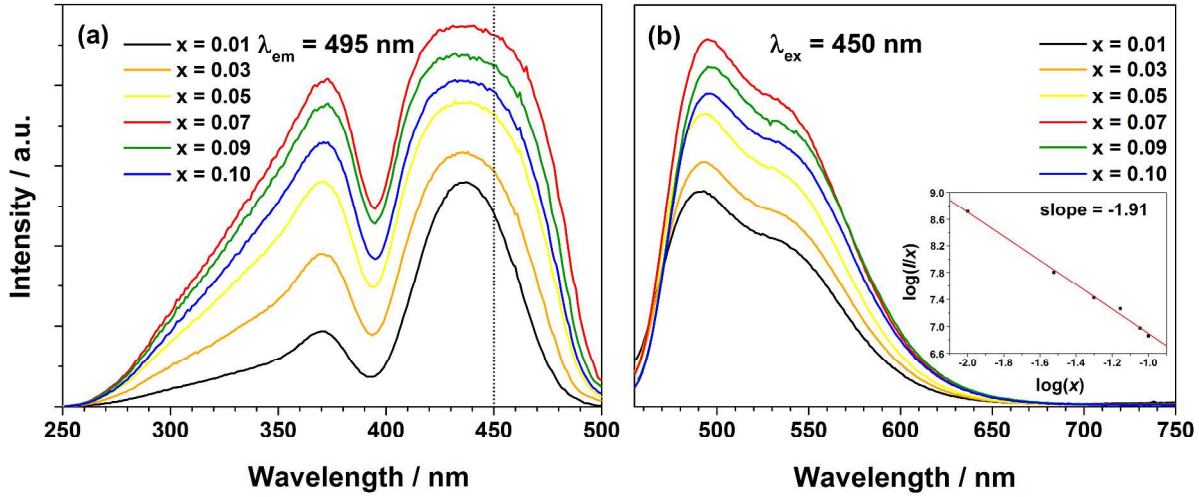

Figure 4 (a) PLE spectra (monitored at λ_{em} = 495 nm) and (b) PL spectra (λ_{ex} = 450 nm) of $Ca(Y_{1-x}Ce_x)_2Si_2S_8$ with different Ce^{3+} concentration x. The inset shows the correlation between log(I/x) with log(x).

The asymmetric emission band in the PL spectrum is fitted into good approximation with two Gaussian curves centered at 491 nm (20,366 cm^{-1}) and 545 nm (18,348 cm^{-1}), which can be ascribed to the transitions from the lowest 5*d* level to the two $^2F_{7/2}$ and $^2F_{5/2}$ ground states of the Ce^{3+} ions.[33] Then, the energy gap between $^2F_{7/2}$ and $^2F_{5/2}$ associated with spin-orbit coupling is calculated to be 2018 cm^{-1} (250 meV). On the other hand, the PLE spectrum is characterized by two main excitation bands in the UV−Vis range: one band in the UV region, peaking at ~370 nm (ranging from 250 to 400 nm) and the other band in the visible region at ~430 nm (range from 400 to 500 nm). The PLE and PL spectra of $Ca(Y_{1-x}Ce_x)_2Si_2S_8$ (x = 0.01, 0.03, 0.05, 0.07, 0.09, and 0.10) are shown in Figure 4. The relative intensity in both PLE and PL spectra varies with the Ce^{3+} dopant concentration, and an optimal value of x = 0.07 (ca. 7 mol %) is obtained for the critical concentration (x_c). Because each activator ion is introduced solely into one site, there is one activator per V/x_cN on average when considering the concentration quenching caused by energy transfer mechanisms such as exchange interaction, radiation reabsorption, or multipole−multipole interaction.[34] The critical energy transfer distance (R_c) is approximately equal to twice the radius of a sphere with the volume:[35,36]

$$R_c \approx 2\left(\frac{3V}{4\pi x_c N}\right)^{\frac{1}{3}}$$

(1) where V represents the volume of the unit cell, x_c is the critical dopant concentration, and N is the number of total Ce^{3+} sites in the unit cell. In this case, V = 1819.83 Å^3, N = 6, and x_c = 0.14 (ca. 7 mol %). Thus, the R_c of Ce^{3+} was calculated to be 16.05 Å. If rapid migration of Ce^{3+} ions occurs, quenching tends to be proportional to the Ce^{3+} concentration, which is not indicated in the PL spectra. Since the exchange interaction generally takes place in the forbidden transition (R_c is typically ~5 Å), the PLE and PL spectra do not overlap well. Therefore, we can infer that the nonradiative concentration quenching between two nearest Ce^{3+} centers occurs via electric multipolar interactions based on the Dexter theory.[37] For the emission intensity per activator concentration, the following equation can be described:[38]

$$\frac{I}{x} = \frac{k}{1+\beta(x)^{\theta/3}}$$

(2) where I represents the quenching intensity; x represents the Ce^{3+} concentration; k and β represent constants for individual electric multipolar interactions; θ = 6, 8, and 10 correspond to dipole−dipole, dipole−quadrupole, and quadrupole−quadrupole integrations, respectively. As represented in Figure 4 (b), the correlation between log(I/x) and log(x) can be fitted linearly within the PL spectra of $Ca(Y_{1-x}Ce_x)_2Si_2S_8$ (x = 0.01, 0.03, 0.05, 0.07, 0.09, and 0.10) and the θ value is determined to be 5.73 from the slope (θ/3). In particular, the calculated value for $Ca(Y_{1-x}Ce_x)_2Si_2S_8$ is close to 6, which implies that the concentration quenching mechanism in Ce^{3+} emission is strongly accounted for by the dipole−dipole interaction. With increasing Ce^{3+} concentration, the wavelengths of the excitation and emission bands remain practically unchanged for the phosphor material. The full width at half-maximum (FWHM) of the emission band is found to be larger than 150 nm (66,667cm^{-1}). These results depict that the Ce^{3+}-doped $CaY_2Si_2S_8$ thiosilicate phosphor may afford good color rendering when incorporated into pc-WLEDs.

3.3. Quantum Efficiencies and Time-Resolved PL Properties of the $Ca(Y_{1-x}Ce_x)_2Si_2S_8$ Thiosilicate Phosphor

As seen in Figure 5, the absorption of Ce^{3+} increases with increasing Ce^{3+} concentration and reaches a saturation point of ~81% at about x ≥0.05, which is in good agreement with the estimated Ce^{3+} solubility limit for $Ca(Y_{1-x}Ce_x)_2Si_2S_8$. The external quantum efficiency (QE_{ext}) results show relative corresponding characteristics with the $4f^1 \rightarrow 5d^1$ transition observed in the PLE spectra. At low Ce^{3+} concentrations, with an increase in absorption, the QE_{ext} value for $Ca(Y_{1-x}Ce_x)_2Si_2S_8$ increases as expected from x = 0.01 to 0.10 and reaches maximum values of about 46.59% and 44.87% at x = 0.07, under excitation at 430 and 450 nm, respectively. When x >0.07, the QE_{ext} significantly decreases, mainly due to Ce^{3+} concentration quenching, which in turn results from Ce^{3+}−Ce^{3+} interactions.

Furthermore, the decay curves of $Ca(Y_{1-x}Ce_x)_2Si_2S_8$ (x = 0.01, 0.03, 0.05, 0.07, and 0.10) phosphors excited at 450 nm and monitored at 495 nm are shown in Figure 6. The corresponding luminescence decay lifetimes can be calculated to be 51.83, 48.16, 46.81, 43.41, and 39.99 ns, using the first-order exponential equation.[39]

$$I = I_o \exp\left(\frac{-t}{\tau}\right) \quad (3)$$

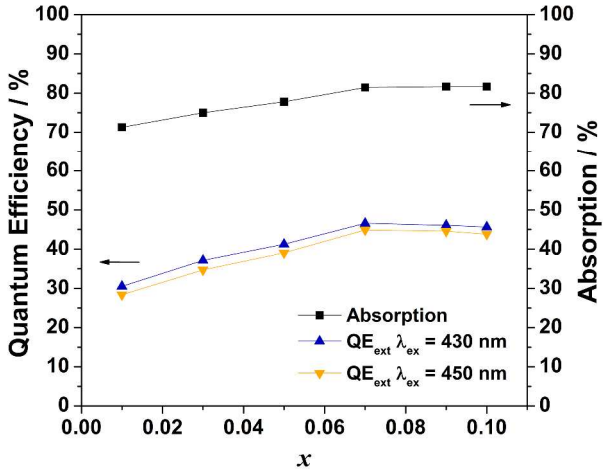

Figure 5 Absorption and external quantum efficiency (QE_{ext}) as a function of x in $Ca(Y_{1-x}Ce_x)_2Si_2S_8$ under excitation at 430 and 450 nm, respectively.

where I and I_0 are the luminescence intensities at time t and 0, respectively, and τ is the decay lifetime. The lifetime of Ce^{3+} in $Ca(Y_{1-x}Ce_x)_2Si_2S_8$ is on the order of nanoseconds, which is also reasonable for the $5d^1 \rightarrow 4f^1$ transitions of Ce^{3+} and similar to that usually observed.[40–42] With increasing Ce^{3+} concentration, both the Ce^{3+}–Ce^{3+} energy transfer rate and the probability of energy transfer to quenching sites increase; as a result, the lifetime shortens with increasing Ce^{3+} concentration. However, due to the longer Y–Y distance (~5.1 Å) in $Ca(Y_{1-x}Ce_x)_2Si_2S_8$, a low energy transfer rate between Ce^{3+} ions may result; thus, there is no notable change in the lifetime with variations in the Ce^{3+} concentration in $Ca(Y_{1-x}Ce_x)_2Si_2S_8$. Moreover, the good fitting results by exponential decay with a single component illustrate that the Ce^{3+} ions occupy only one site in the $CaY_2Si_2S_8$ host, which is consistent with $Ca(Y_{0.93}Ce_{0.07})_2Si_2S_8$ and the PL spectra shown in Table 1 and Figure 4 (b), respectively.

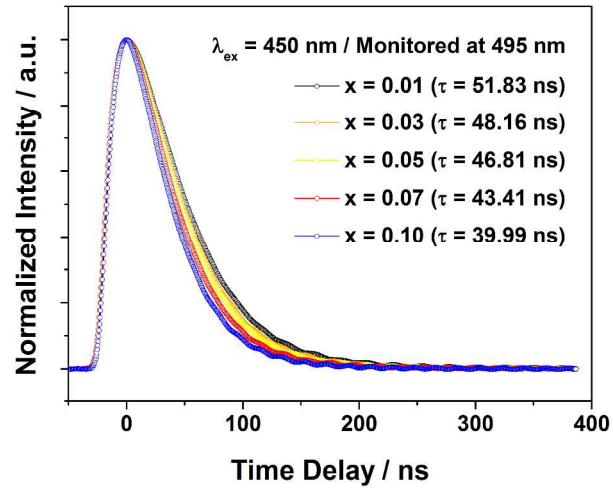

Figure 6 Decay curves of $Ca(Y_{1-x}Ce_x)_2Si_2S_8$ (x = 0.01, 0.03, 0.05, 0.07, and 0.10) phosphors under 450 nm excitation and monitored at 495 nm.

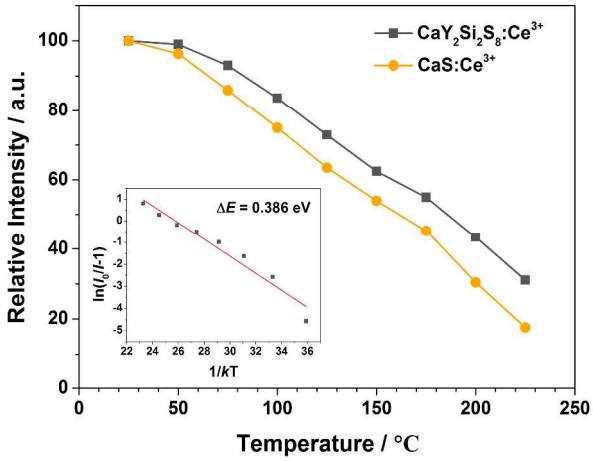

Figure 7 Temperature-dependent PL intensity of $CaY_2Si_2S_8:Ce^{3+}$ and $CaS:Ce^{3+}$. The inset shows the fitted PL intensity and the calculated thermal activation energy (E_a) as a function of temperature.

3.4. Temperature-Dependent PL Properties and Time-Dependent PL Properties of the $Ca(Y_{1-x}Ce_x)_2Si_2S_8$ Thiosilicate Phosphor

Figure 7 shows the temperature-dependent PL intensity of $CaY_2Si_2S_8:Ce^{3+}$ and $CaS:Ce^{3+}$ in the range of 20 to 230 °C. The PL intensity of both samples is diminished as compared to that observed at room temperature, which may be rationalized by the fact that increasing temperature increases the population of higher vibration levels, the density of phonons, and the probability of nonradiative transfer.[43] Depending on the PL results, the intensity of thiosilicate is comparable to (or more stable than) that of binary sulfides. To investigate the origin of the temperature-dependent emission intensity, the activation energy (E_a) of the electrons excited from the $4f$ level to the lowest $5d$ level of Ce^{3+} can be described in following equation:[43]

$$I(T) = \frac{I_o}{1 + A\exp(-\frac{E_a}{kT})} \quad (4)$$

where I_0 and $I(T)$ represent the PL intensity at room temperature and testing temperature (20–230 °C), respectively, and k is the Boltzmann constant. The value of E_a for $CaY_2Si_2S_8:Ce^{3+}$ was estimated to be 0.386 eV as shown in the inset in Figure 7. In addition, for application in higher-powered LEDs, chemical stability of the phosphor is an important parameter to be considered. Figure 8 presents the time-dependent PL intensity of $CaY_2Si_2S_8:Ce^{3+}$ exposed to ambient air. The PL intensity of $CaY_2Si_2S_8:Ce^{3+}$ drops only by ~20% upon exposure to ambient air for 5 weeks. This observation indicates that the $CaY_2Si_2S_8:Ce^{3+}$ thiosilicate phosphor is mostly stable against degradation under ambient conditions.

3.5. Performance of LED Devices Based on the $Ca(Y_{1-x}Ce_x)_2Si_2S_8$ Thiosilicate Phosphor

To demonstrate the potential of $Ca(Y_{1-x}Ce_x)_2Si_2S_8$ for pc-WLEDs application, the $Ca(Y_{0.93}Ce_{0.07})_2Si_2S_8$ phosphor was utilized to

fabricate a white LED with red-emitting $CaAlSiN_3:Eu^{2+}$[31] commodity and a 450 nm InGaN-based LED chip. When excited by a blue chip, the whole visible spectral region can be obtained from

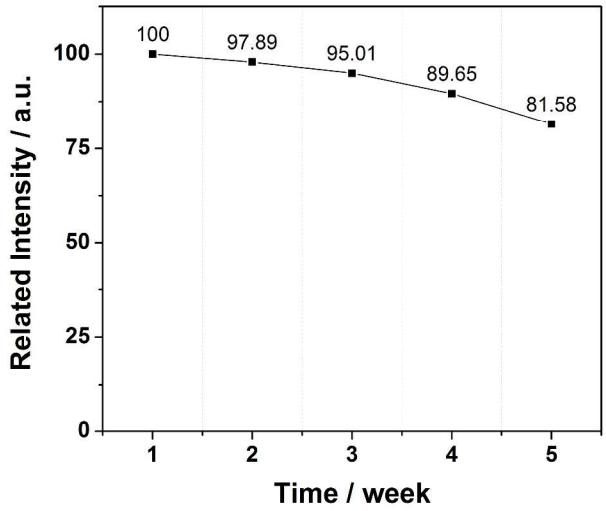

Figure 8 Time-dependent PL intensity of $CaY_2Si_2S_8:Ce^{3+}$ exposed to ambient air.

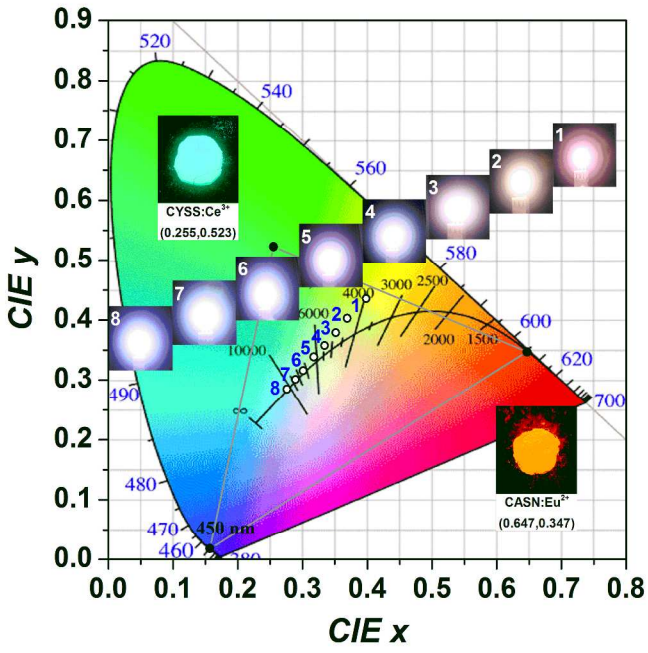

Figure 9 Variation in CIE chromaticity coordinates as a function of phosphor/resin under 350 *m*A driving current. The insets show $CaY_2Si_2S_8:Ce^{3+}$ (up) and $CaAlSiN_3:Eu^{2+}$ (down) phosphor photographs recorded under 365 nm excitation.

blue emission at 450 nm corresponding to the InGaN-based LED chip, broad green emission at 495 nm corresponding to the $Ca(Y_{0.93}Ce_{0.07})_2Si_2S_8$ phosphor, and red emission at 630 nm corresponding to the $CaAlSiN_3:Eu^{2+}$[31] commodity. With increasing ratio of the silicone resin content, the color tone and CIE color coordinates of the trichromatic LED devices could be tuned from orange (point (1), (0.3985, 0.4347)) through white (point (5), (0.3175, 0.3384)), and eventually cool white (point (8), (0.2758, 0.2847)), as shown in Figure 9 and Table 1, respectively. The inset of Figure 9 shows photographs of the LED packaging turned on under a forward bias of 350 *m*A.

Figure 10 shows the EL spectra of InGaN-based white LED device under different driving currents in the range 150–850 *m*A and

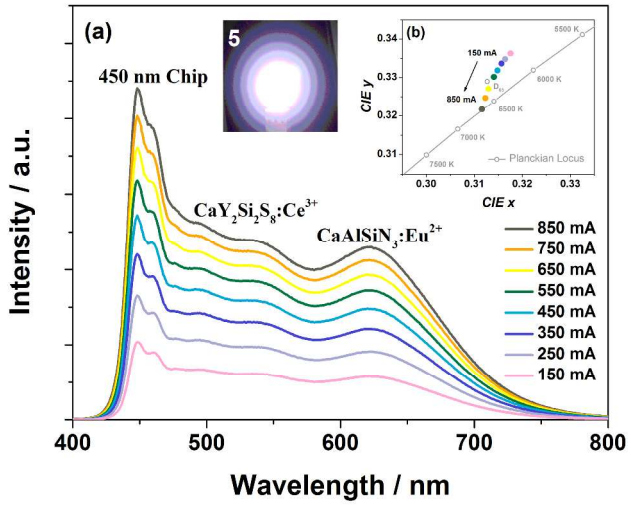

Figure 10 (a) EL spectra of the device using $CaY_2Si_2S_8:Ce^{3+}$ + red phosphor + 430 nm LED chip and (b) variation in CIE chromaticity coordinates of WLED operated under different currents (150−850 *m*A). The inset shows the corresponding LED device photograph.

Table 2 summarizes the optical properties of the $Ca(Y_{0.93}Ce_{0.07})_2Si_2S_8$-based white LED device. The EL intensity of the blue, green, and red bands of the white LED device increased while increasing the forward-biased current from 150 to 850 *m*A, and the saturation phenomenon was not observed even at a high forward current of 850 *m*A. As shown in the inset of Figure 10, with an increase in the driving current, the CIE chromaticity coordinates shifted slightly from (0.3176, 0.3363) to (0.3116, 0.3217). The results demonstrated the excellent color stability of the $Ca(Y_{0.93}Ce_{0.07})_2Si_2S_8$ thiosilicate phosphor with different driving currents. In addition, the CCT and CRI values increased from 6207 K to 6629 K and from 94.28 to 92.62, respectively, with an increase in driving current from 150 to 850 *m*A.

Compared with the white LED lamp using a conventional $Y_3Al_5O_{12}:Ce^{3+}$ phosphor having poor CRI values in the range from 70 to 75 and a high color temperature of >8000 K,[1,44–46] the generated white light in this work possesses rather improved properties, higher CRI, and lower color temperature. Given that the overall device performance depends on numerous factors starting with the phosphor manufacturing issues, efficiency of the LED chip, fabrication processes, etc., we believe that the performance of the white LED device can be further enhanced by optimization of the device structure and operation parameters.

4. Conclusions

In summary, a new green-emitting thiosilicate phosphor with the chemical composition $Ca(Y_{1-x}Ce_x)_2Si_2S_8$ (x = 0.01, 0.03, 0.05, 0.07, 0.09, and 0.10) was synthesized and studied. The detailed crystal structure, overall luminescence performance (i.e., PL/PLE intensity, QE), decay lifetime, thermal luminescence quenching behavior, chemical stability, and its application in LED fabrication were investigated. Preliminary studies show that this novel green phosphor is a potential

candidate for white LED, especially for the generation of warm white light.

Table 1 Chromaticity and optical parameters for *pc*-WLEDs with different $Ca(Y_{0.93}Ce_{0.07})_2Si_2S_8$ phosphor/resin weight ratios ($Ca(Y_{0.93}Ce_{0.07})_2Si_2S_8$ is the conversion phosphor layer) under 350 mA driving current

No.	Phosphor/resin weight ratio (%)	CIE *x*	CIE *y*	CCT (K)	CRI (R_a)	Luminous efficiency (lm/W)
1	40	0.3985	0.4357	3896	91.75	10.68
2	35	0.3690	0.4029	4465	92.21	13.90
3	30	0.3511	0.3788	4859	92.87	18.67
4	25	0.3341	0.3575	5438	93.70	24.72
5	20	0.3175	0.3384	6199	94.61	28.63
6	15	0.3007	0.3155	7408	95.14	28.79
7	10	0.2891	0.3008	8662	93.76	31.35
8	5	0.2758	0.2847	10822	92.06	37.02

Table 2 Chromaticity and optical parameters for *pc*-WLEDs with $Ca(Y_{0.93}Ce_{0.07})_2Si_2S_8$ as the conversion phosphor layer under different driving currents (150−850 mA)

Drive Current *I* (mA)	CIE *x*	CIE *y*	CCT (K)	CRI (R_a)	Luminous efficiency (lm/W)
150	0.3176	0.3363	6207	94.28	15.35
250	0.3164	0.3348	6273	94.52	22.24
350	0.3156	0.3337	6319	94.65	28.57
450	0.3148	0.3319	6374	94.58	31.58
550	0.3141	0.3302	6442	94.23	35.11
650	0.3130	0.3271	6496	93.83	37.98
750	0.3123	0.3247	6556	93.51	40.70
850	0.3116	0.3217	6629	92.62	42.92

Acknowledgements

This research was supported by Ministry of Science and Technology of Taiwan (ROC) under Contract No. NSC101-2113-M-009-021-MY3. We thank Dr. Ting-Shan Chan of NSRRC, Taiwan for performing crystal structure refinement, Drs. Hung-Yu Hsu and Hsin-Han Liu for assistance in the helpful suggestions.

Notes and references

[a]Phosphors Research Laboratory, Department of Applied Chemistry and Institute of Molecular Science, National Chiao Tung University, Hsinchu 30010, Taiwan. E-mail: tmchen@mail.nctu.edu.tw.
[b]Material and Chemical Research Laboratories, ITRI, Hsinchu 30011, Taiwan

1 M. R. Krames, O. B. Schekin, R. Mueller-Mach, and M. G. Craford, *J. Disp. Technol.*, 2007, **3**, 160−175.
2 H. S. Jang, H. Yang, S. W. Kim, J. Y. Han, S. -G. Lee, and D. Y. Jeon, *Adv. Mater. (Deerfield Beach Fla.)*, 2008, **20**, 2696−2702.
3 Y. Narukawa, M. Sano, M. Ichikawa, S. Minato, and T. Mukai, *Jpn. J.Appl. Phys.*, Part 2, 2007, **46**, L963−L965.
4 B. Damilano, P. Demolon, J. Brault, T. Huault, F. Natali, and J. Massies, *J. Appl. Phys.*, 2010, **108**, 073115.
5 S. Ye, F. Xiao, Y. X. Pan, Y. Y. Ma, and Q. Y. Zhang, *Mater. Sci. Eng., R*, 2010, **71**, 1−34.
6 T. G. Kim, H. S. Lee, C. C. Lin, T. Kim, R. S. Liu, T. S. Chan, and S. J. Im, *Appl. Phys. Lett.*, 2010, **96**, 061904.
7 J. S. Kim, P. E. Jeon, J. C. Choi, and H. L. Park, *Appl. Phys. Lett.*, 2004, **84**, 2931−2933.
8 J. K. Park, M. A. Lim, C. H. Kim, and H. D. Park, *Appl. Phys. Lett.*, 2003, **82**, 683−685.
9 Y. Uchida and T. Taguchi, *Opt. Eng.*, 2005, **44**, 124003.
10 Y. -C. Chiu, W. -R. Liu, C. -K. Chang, C. -C. Liao, Y. -T. Yeh, S. -M. Jang, and T. -M. Chen, *J. Mater. Chem.*, 2010, **20**, 1755−1758.
11 N. Narendran, Y. Gu, J. P. Freyssinier, H. Yu, and L. Deng, *J. Cryst. Growth*, 2004, **268**, 449−456.
12 J. L. Wu, G. Gundiah, and A. K. Cheetham, *Chem. Phys. Lett.*, 2007, **441**, 250−254.
13 P. Dorenbos, *J. Lumin.*, 2000, **91**, 91−106.
14 P. Dorenbos, *J. Lumin.*, 2000, **91**, 155−176.
15 W. B. Im, K. Page, S. P. DenBaars, and R. Seshadri, *J. Mater. Chem.*, 2009, 19, 8761−8766.
16 Y. F. Liu, X. Zhang, Z. D. Hao, X. J. Wang, and J. H. Zhang, *J. Mater. Chem.*, 2011, **21**, 6354−6358.
17 Y. Nanai, Y. Sakamoto, and T. Okuno, *Jpn. J. Appl. Phys.*, 2013, **52**, 04CG15.
18 Z. Xia, J. Zhou, and Z. Mao, *J. Mater. Chem. C*, 2013, **1**, 5917−5924.
19 Y. Q. Li, J. E. J. van Steen, J. W. H. van Krevel, G. Botty, A. C. A. Delsing, F. J. DiSalvo, G. de With, and H. T. Hintzen, *J. Alloys Compd.*, 2006, **417**, 273−279.
20 V. Bachmann, C. Ronda, O. Oeckler, W. Schnick, and A. Meijerink, *Chem. Mater.*, 2009, **21**, 316−325.
21 P. F. Smet, N. Avci, B. Loos, J. E. Van Haecke, and D. Poelman, *J. Phys.: Condens. Matter*, 2007, **19**, 246223.
22 P. F. Smet, K. Korthou, J. E. Van Haecke, and D. Poelman, *Mater. Sci. Eng. B*, 2008, **146**, 264.
23 A. B. Parmentier, P. F. Smet, F. Bertram, J. Christen, and D. Poelman, *J. Phys. D*, 2010, **43**, 085401−085407.
24 P. F. Smet, I. Moreels, Z. Hens, and D. Poelman, *Materials*, 2010, **3**, 2834−2883.
25 A. B. Parmentier, P. F. Smet, and D. Poelman, *Opt. Mater.*, 2010, **33**, 141−144.
26 M. Nishimura, Y. Nanai, T. Bohda, and T. Okuno, *Jpn. J. Appl. Phys.*, 2009, **48**, 072301.
27 M. Sugiyama, Y. Nanai, Y. Okada, and T. Okuno, *J. Phys. D*, 2011, **44**, 095404.

28 Y. Nanai, C. Sasaki, Y. Sakamoto, and T. Okuno, *J. Phys. D*, 2011, **44**, 405402.
29 Y. Nanai, Y. Sakamoto, and T. Okuno, *J. Phys. D*, 2012, **45**, 265102.
30 M. Daszkiewicza, O. V. Marchukb, L. D. Gulayc, and D. J. Kaczorowski, *J. Alloys Compd.*, 2012, **519**, 85−91.
31 K. Uheda, N. Hirosaki, Y. Yamamoto, A. Naito, T. Nakajima, and H. Yamamoto, *Electrochem. Solid-State Lett*., 2006, **9**, H22−H25.
32 S. -P. Lee, C. -H. Huang, T. -S. Chan, and T. -M. Chen, *ACS Appl. Mater. Interfaces*, 2014, **6**, 7260−7267.
33 N. Kodama, M. Yamaga, and B. J. Henderson, *Appl. Phys.*, 1998, **84**, 5820−5822.
34 Y. -C. Wu, D. -Y. Wang, T. -M. Chen, C. -S. Lee, K. -J. Chen, and H. -C. Kuo, *ACS Appl. Mater. Interfaces*, 2011, **3**, 3195−3199.
35 G. Blasse, *Philips Res. Rep.*, 1969, **24**, 131−144.
36 M. M. Shang, G. G. Li, X. J. Kang, D. M. Yang, D. L. Geng, and J. Lin, *ACS Appl. Mater. Interfaces*, 2011, **3**, 2738−2746.
37 D. L. Dexter, *J. Chem. Phys.*, 1953, **21**, 836−850.
38 L. G. Van Uitert, *J. Electrochem. Soc.*, 1967, **114**, 1048−1053.
39 R. Pang, C. Li, L. Shi, and Q. Su, *J. Phys. Chem. Solids*, 2009, **70**, 303−306.
40 C. -H. Huang and T. -M. Chen, *J. Phys. Chem. C*, 2011, **115**, 2349–2355.
41 V. Bachmann, C. Ronda, and A. Meijerink, *Chem. Mater.*, 2009, **21**, 2077−2084.
42 Y. Liu, J. Hao, W. Zhuang, and Y. Hu, *J. Phys. D: Appl. Phys.*, 2009, **42**, 245102−245108.
43 R. -J. Xie, N. Hirosaki, N. Kimura, K. Sakuma, and M. Mitomo, *Appl. Phys. Lett.*, 2007, **90**, 191101.
44 V. Bachmann, C. Ronda, and A. Meijerink, *Chem. Mater.*, 2009, **21**, 2077−2084.
45 R. Mueller-Mach, G. Mueller, M. R. Krames, H. A. Höppe, F. Stadler, W. Schnick, T. Juestel, and P. Schmidt, *Phys. Status Solidi A*, 2005, **202**, 1727−1732.
46 A. A. Setlur, W. J. Heward, M. E. Hannah, and U. Happek, *Chem. Mater.*, 2008, **20**, 6277−6283.

$CaY_2Si_2S_8:Ce^{3+}$: A novel green-emitting thiosilicate phosphor for white light-emitting diodes

Szu-Ping Lee, Chien-Hao Huang, and Teng-Ming Chen*

Graphical Abstract

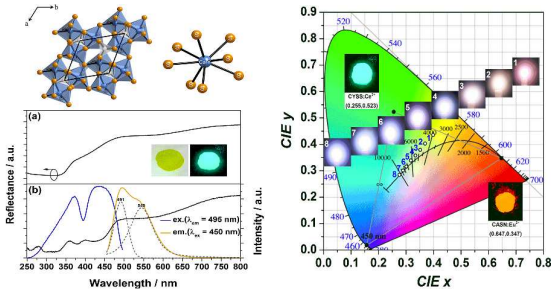

The luminescence of a green-emitting $CaY_2Si_2S_8:Ce^{3+}$ phosphor and its applicability in fabrication of white-LEDs with high CRI and varied CCTs were explored.